Spiro[4.4]nonatetraene and its Positive and Negative Radical Ions: Molectronic Structure Investigations

by **Edwin Haselbach**, **Michael Allan***, **Thomas Bally***, **Pawel Bednarek**, and **Anne-Christelle Sergenton**

Institut de Chimie Physique, Université de Fribourg, Pérolles, CH-1700 Fribourg

and **Armin de Meijere** and **Sergej Kozhushkov**

Institut für Organische Chemie der Georg-August-Universität, Tammannstrasse 2, D-37077 Göttingen

and **Manuel Piacenza** and **Stefan Grimme**

Organisch-Chemisches Institut, Westfälische Wilhelms-Universität, Corrensstrasse 40, D-48149 Münster

Dedicated to *Edgar Heilbronner* on the occasion of his 80th birthday

The electronic structure of spiro[4.4]nonatetraene **1** as well as that of its radical anion and cation were studied by different spectroscopies. The electron-energy-loss spectrum in the gas phase revealed the lowest triplet state at 2.98 eV and a group of three overlapping triplet states in the 4.5 – 5.0 eV range, as well as a number of valence and *Rydberg* singlet excited states. Electron-impact excitation functions of pure vibrational and triplet states identified various states of the negative ion, in particular the ground state with an attachment energy of 0.8 eV, an excited state corresponding to a temporary electron attachment to the $2b_1$ MO at an attachment energy of 2.7 eV, and a core excited state at 4.0 eV. Electronic-absorption spectroscopy in cryogenic matrices revealed several states of the positive ion, in particular a richly structured first band at 1.27 eV, and the first electronic transition of the radical anion. Vibrations of the ground state of the cation were probed by IR spectroscopy in a cryogenic matrix. The results are discussed on the basis of density-functional and CASSCF/CASPT2 quantum-chemical calculations. In their various forms, the calculations successfully rationalized the triplet and the singlet (valence and *Rydberg*) excitation energies of the neutral molecule, the excitation energies of the radical cation, its IR spectrum, the vibrations excited in the first electronic absorption band, and the energies of the ground and the first excited states of the anion. The difference of the anion excitation energies in the gas and condensed phases was rationalized by a calculation of the *Jahn-Teller* distortion of the anion ground state. Contrary to expectations based on a single-configuration model for the electronic states of **1**, it is found that the gap between the first two excited states is different in the singlet and the triplet manifold. This finding can be traced to the different importance of configuration interaction in the two multiplicity manifolds.

1. Introduction. – Spiroconjugation, a concept first introduced in 1967 [1][2], results in many interesting spectroscopic and chemical properties. As a consequence, spiroconjugated compounds have often been studied experimentally and theoretically, and they find applications in technology (*e.g.*, as materials for organic light-emitting diodes [3] or nonlinear optical materials).

1
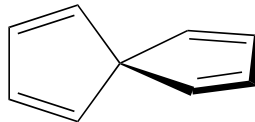
Spiro[4.4]nonatetraene **1** is a prototypical example of a pair of π-systems experiencing interaction *via* a central spiro linkage. As such, it has attracted the attention of both experimentalists [4 – 9] and theoreticians [1] [2] [6] [10 – 13]. *Simmons* and *Fukanaga* [1] and *Hoffmann et al.* [2] first established qualitative orbital diagrams for **1** on the basis of orbital interactions between the two cyclopentadiene moieties. Based on symmetry considerations, they noted that spiroconjugation for molecules like **1** results in a splitting of the cyclopentadiene HOMOs, whereas it leaves the LUMOs degenerate. As a consequence, the first electronic absorption (EA) band of cyclopentadiene was predicted to be split into a lower- and a higher-lying component of very different absorptivity in **1**.

After the synthesis of **1** had been achieved [4], this prediction was confirmed experimentally [5]. In fact, the EA spectrum of **1** (λ_{max} 276 and 218 nm) permitted a first tentative assessment of the magnitude of the above MO splitting due to spiroconjugation (1.23 eV). A year later, *Heilbronner* and co-workers [6] reported the photoelectron (PE) spectrum which showed exactly the same splitting between the two highest occupied MOs. They demonstrated that this is no coincidence but that, due to its high symmetry and the almost perfect pairing properties of its π-MOs, **1** is a rare case where the difference in the first two excitation energies should indeed be equal to the difference between the first two ionization energies. As will be explained in *Sect. 2*, this is due to the cancellation of certain electron repulsion and exchange integrals.

In principle, those properties of **1** which led to the above-mentioned simple relationship between ionization and excitation energies should also make this compound amenable to a direct comparison of the HOMO → LUMO excitation energies in the singlet, the triplet, the radical cation, and the radical anion manifold of states[1]), as it was proposed [14] and applied some time ago by one of the present authors [15]. A test of the applicability of this so-called 'SDT rule' (where SDT stands for singlet, doublet, triplet) to **1** requires, apart from the known singlet-singlet HOMO → LUMO excitation energy of *ca.* 4.5 eV [4] [6], also the knowledge of the singlet-triplet and the doublet-doublet HOMO → LUMO excitation energies[1]).

We therefore set out to determine these quantities both experimentally and theoretically. The singlet and triplet excitation energies of **1**, as well as the ground and excited states of the radical anion **1**[·−] were investigated by electron-energy-loss (EEL) spectroscopy in the gas phase. Doublet-doublet transitions of both **1**[·−] and the radical cation **1**[·+] were measured by electronic-(photo)absorption spectroscopy of these species generated radiolytically in solid matrices at low temperatures. The transition energies were then modelled by means of CASPT2, DFT/MRCI, and the TD-DFT methods (see *Exper. Part*). To set the stage required to put these findings into proper perspective, we will precede the experimental results with a presentation of the electronic structure of **1** and its radical ions within the conceptual framework proposed by *Heilbronner* and co-workers [6].

2. The Electronic Structure of 1. – Different authors have shown how the relevant π MOs of **1** depicted in *Fig. 1* can be constructed as linear combinations of the π MOs of

---

[1])   Note that, for simplicity, we use the terms HOMO and LUMO as defined for neutral **1** (*i.e.,* the $1a_2$ and $8e$ orbitals, resp., in *Fig. 1*) also for the radical anion, despite the fact that the 'LUMO' is singly occupied in **1**[·−]).

cyclopentadiene [1][2][6]. In their analysis of the electronic structure of **1**, *Heilbronner* and co-workers derived qualitative π MOs by forming linear combinations of π and π^* MOs centered at each of the double bonds of **1** (LCBO model). As a starting point, let us reiterate briefly how these authors showed that the difference between the first two *ionization* energies $\Delta I(2,1)$ should be equal to the difference between the first two *excitation* energies $\Delta E(2,1)$ in **1**. We will use the same orbital numbering as *Heilbronner* and co-workers, given in bold numbers in *Fig. 1*.
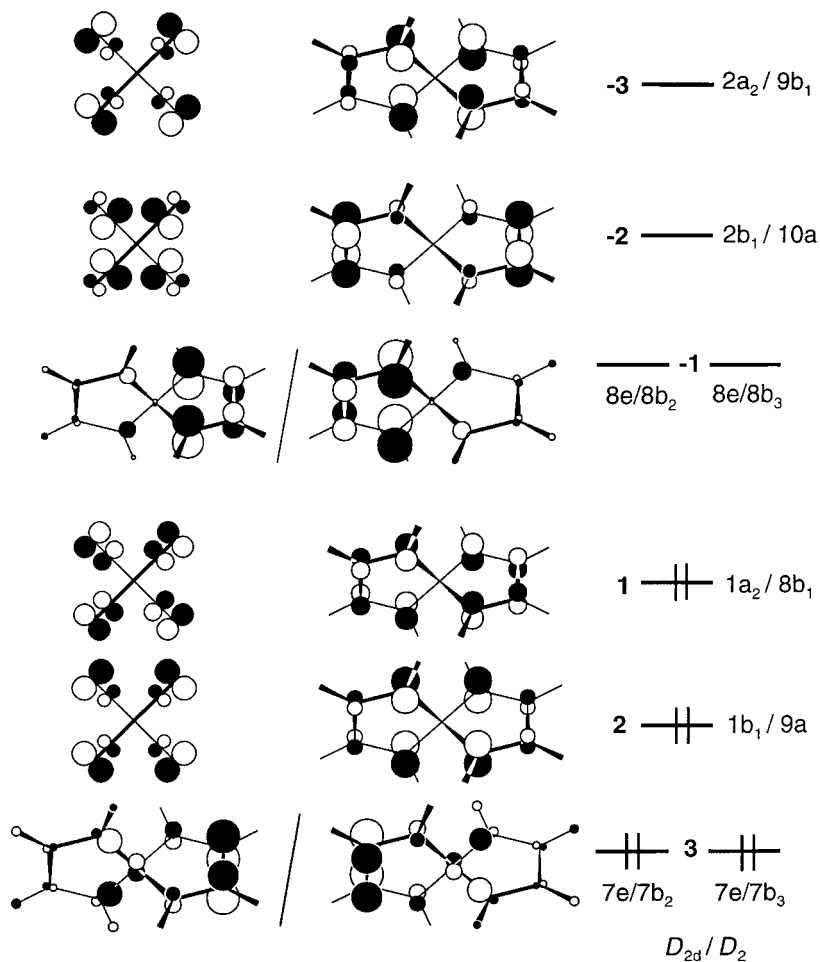
Fig. 1. *MOPLOT Representation of the molecular orbitals* (MOs) *of* **1** *as obtained from a HF/3-21G calculation.* On the left, the nondegenerate MOs are additionally shown in a view along the long axis of the molecule, to highlight the spiro-conjugative properties prevailing in **1**. The symmetry labels in *Fig. 1* are given both for the D_{2d} and for the D_2 point group, the latter being required in **1**$^{.-}$, which is subject to *Jahn-Teller* distortion. The bold numbers refer to the numbering of MOs used by *Heilbronner* and co-workers [6] and employed in the present discussion (*Sects. 2* and *4*).

According to *Koopmans*' theorem, $\Delta I(2,1)$ is simply equal to the energy difference of the two orbitals from which the first two ionizations occur, *i.e.*, $\Delta I(2,1) = -\Delta\varepsilon(2,1) = \varepsilon_2 - \varepsilon_1$. Following standard conventions, $\Delta E(2,1)$ (*i.e.*, the energy difference of the excitations that correspond to $1 \rightarrow -1$ and to $2 \rightarrow -1$ electron promotion) for singlet and triplet states can be expressed by *Eqns. 1* and *2*, where the *J*s and *K*s are the *Coulomb* and exchange integrals, respectively (see *Eqns. 3* and *4*, resp.). *Heilbronner* and co-workers demonstrated that, within the above LCBO model of **1** and on the basis of the ZDO approximation, $J_{1,-1} = J_{2,-1}$ and $K_{1,-1} = K_{2,-1}$, and hence *Eqn. 5* followed, which explained their observation of equal gaps between the first two excited singlet states and the first two ionization energies. At the time, *Heilbronner* and co-workers did not have the necessary experimental data available to examine whether the first part of *Eqn. 5*, *i.e.*, $\Delta^3 E(2,1) = \Delta^1 E(2,1)$ also holds.

$$\Delta^1 E(2,1) = \Delta I(2,1) - (J_{1,-1} - J_{2,-1}) + 2(K_{1,-1} - K_{2,-1}) \tag{1}$$

$$\Delta^3 E(2,1) = \Delta I(2,1) - (J_{1,-1} - J_{2,-1}) \tag{2}$$

$$J_{1,-1} = \langle \Psi_1^2(1) \,|\, e^2/r_{12} \,|\, \Psi_{-1}^2(2) \rangle \tag{3}$$

$$K_{1,-1} = \langle \Psi_1(1)\Psi_{-1}(1) \,|\, e^2/r_{12} \,|\, \Psi_1(2)\Psi_{-1}(2) \rangle \tag{4}$$

$$\Delta^3 E(2,1) = \Delta^1 E(2,1) = \Delta I(2,1) \tag{5}$$

Furthermore, if *Eqn. 5* would also hold for the triplet states, then, according to the SDT rule [14], the excitations which correspond to HOMO $\rightarrow$ LUMO $(1 \rightarrow -1)$ electron promotion in the radical cation **1**$^{\cdot+}$ and the radical anion **1**$^{\cdot-}$ should lie at the geometric mean of the corresponding excitation in ^{1}**1** and ^{3}**1**, *i.e.* $^2E(1 \rightarrow -1) = [^1E(1 \rightarrow -1) \cdot {}^3E(1 \rightarrow -1)]^{1/2}$. It is the purpose of this work to examine these relationships by providing the corresponding experimental data which are presented in *Sect. 3*.

3. Results and Discussion. – 3.1. *Electronic Structure of* **1**: *Singlet and Triplet States.* Two representative electron-energy-loss (EEL) spectra are shown in *Fig. 2* (additional spectra were recorded at other residual energies [16] but are not shown here). The top spectrum (*Fig. 2,a*), recorded at the residual energy $E_r = 20$ eV, is representative of dipole- and spin-allowed transitions. The lower spectrum (*Fig. 2,b*), recorded at the residual energy $E_r = 1.1$ eV, is dominated by spin-forbidden (singlet-triplet) transitions; the spin- and dipole-allowed transitions appear only weakly. The band peaking at 2.98 eV in the *Fig. 2,b* must therefore be due to HOMO $\rightarrow$ LUMO excitation to yield the lowest triplet state, and the first band at 4.46 eV in *Fig. 2,a* due to a transition to the corresponding singlet state. The latter assignment follows that given previously [5][6] for the UV-absorption spectra.

Additional information on the nature of the observed transitions comes from the band shape: bands arising from transitions to *Rydberg* states converging to a given ionization energy have vibronic profiles resembling closely the profile of the corresponding photoelectron band. The sharply structured band with 0-0 transition
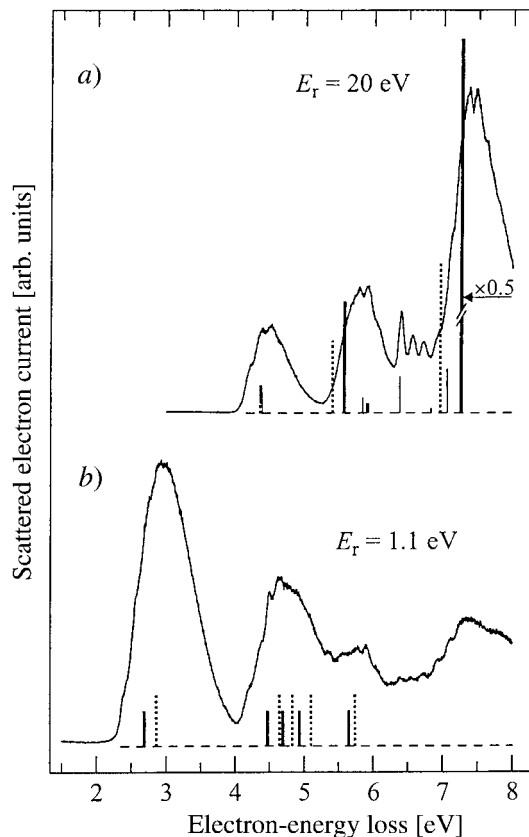
Fig. 2. *Electron-energy-loss spectra of* **1**: a) *dipole-allowed transitions, and* b) *singlet-triplet transitions.* The results of DFT-MRCI calculations are indicated by solid vertical lines. The heights of the lines in *Fig. 2,a* indicate the calculated oscillator strengths (transitions with very small or zero oscillator strengths are not shown, but are listed in *Table 2*). Valence transitions are indicated by bold lines, *Rydberg* transitions by thin lines. Results of CASPT2 calculations (valence only) are indicated by dotted lines.
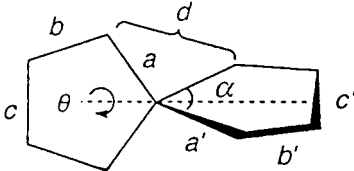
at 6.4 eV in *Fig. 2,a* closely resembles the first photoelectron band of **1**, indicating a *Rydberg* state.

The band peaking around 4.6 eV in the *Fig. 2,b* closely resembles the 4.46 eV singlet band in *Fig. 2,a*. The fact that this band remains intense even under 'triplet conditions', that is when recorded with low residual electron energies, indicates that it cannot be due to the 4.46 eV singlet state alone, and that one or possibly several triplet states are present around this energy. The relative intensities of transitions to different triplet states vary with residual energy, which permits us to learn more about possible overlapping triplet states by recording spectra at different residual energies. In the present case, these results provide evidence [16] for three triplet states in the 4–5 eV range. Only the first vibronic feature (0-0 transition) could be identified for the first two states, at 4.48 and at 4.52 eV. The third band appears as an enhancement of signal intensity at *ca.* 5 eV in spectra recorded with residual energies of *ca.* 3 eV. Spectral

subtraction indicates that this transition peaks at *ca.* 4.9 eV. The presence of a triplet state around this energy is also indicated by the shape of its excitation function recorded at an energy loss of 5.0 eV, shown in *Fig. 3,d*.

Comparison with calculated excitation energies at the B3LYP/6-31G* optimized geometry of **1** (see *Table 1*), as given in *Tables 2* and *3*, permits a more detailed assignment of the spectra. We base the following discussion mainly on the DFT-MRCI results, which have proven in the past to be very useful in assigning EEL spectra [17–19]. The correspondence of the calculated and observed transitions is based on three criteria: *a*) transition energies, *b*) calculated oscillator strengths for the dipole-allowed transitions, and *c*) the *Rydberg* character of a state (derived from the calculated spatial extent of the excited-state wave function and inferred from the observed band shape).

Table 1. *B3LYP/6-31G* Geometries of **1** and Different States of **1**$^{·+}$ and **1**$^{·-}$*. Distances in Å, angles in degrees.

		$a(a')$	$b(b')$	$c(c')$	$d(d')$	$\alpha(\alpha')$	θ
1	(D_{2d},$^1A_1$)	1.522	1.346	1.473	2.546	101.8	90.0
1$^{·+}$	(D_{2d},$^2A_2$)	1.506	1.374	1.439	2.509	102.9	90.0
1$^{·+}$	(D_{2d},$^2B_1$)	1.539	1.364	1.447	2.588	99.9	90.0
1$^{·-}$	(D_2,$^2B_1$)	1.534	1.374	1.444	2.530	100.4	78.7
					(2.620)		
1$^{·-}$	(C_{2v},$^2B_1$)	1.558	1.402	1.415	2.576	100.8	90.0
		(1.530)	(1.348)	(1.479)		(99.8)	

The assignment of the lowest singlet band peaking at 4.46 eV to the HOMO → LUMO ($1a_2 \rightarrow 8e$) transition is confirmed by the excellent agreement with the calculated value of 4.36 eV. This excitation energy is slightly lower than those reported by *Semmelhack* and co-workers [5] (4.49 eV, hexane) and by *Heilbronner* and co-workers [6] (4.53 eV, gas phase; 4.61 eV, hexane, rigisolve), but the presence of the 1150 cm^{-1} vibronic structure [6] leaves no doubt that the same transition is involved in both experiments. The next calculated transition with substantial oscillator strength is that to the 2^1E state (HOMO-1 → LUMO, $1b_1 \rightarrow 8e$), calculated at 5.57 eV, and can, therefore, be assigned to the second intense band peaking at 5.78 eV. This and the ratio of oscillator strengths of the first two transitions (*ca.* 4) is in agreement with previous assignments based on electronic-absorption spectra [5][6][13]. Again, the peak of the band in the EEL spectrum appears at slightly lower energy than in the absorption spectra obtained in hexane (5.85 eV) or in the gas phase (6.05 eV) [6]. Consequently, the gap between the first and the second excited state ($\Delta E(2,1)$ in *Sect. 2*) is 1.32 eV by EEL spectroscopy.

According to DFT-MRCI, two *Rydberg* states lie between the above two valence excited states, a prediction we cannot verify because the corresponding transitions are

Table 2. *Excited Singlet States of* **1**[a])

Sym.	Type[b])	Excitation(s)	Exper. energy[c])[d])	DFT-MRCI energy[d])	f[e])	%[f])	CASPT2 energy[d])	f[e])	%[fg])	TD-DFT energy[d])	f[e])
1^1A_1	V	(ground state)[c])	(0)	(0)	–		(0)	–		(0)	–
1^1E	V	$1a_2 \rightarrow 8e$	4.46	4.36	0.045	91	4.35	0.014	82	4.09	0.008
1^1A_2	R	$1a_2 \rightarrow 9a_1(R)$		5.19	0	88	–[h])	–		–	–
1^1B_1	R	$1a_2 \rightarrow 8b_2(R)$		5.55	0	78	–[h])	–	–	–	–
2^1E	V	$1b_1 \rightarrow 8e$	5.78	5.57	0.182	87	5.40	0.117	71	5.49	0.061
2^1A_1	V	$1a_2^2 \rightarrow 8e^2$		5.59	0	44	5.78	0	42	–[k])	–
		$+ 1b_1,1a_2 \rightarrow 8e^2$				22			17		
		$+ 1b_1^2 \rightarrow 8e^2$				–			13		
3^1E	R	$1a_2 \rightarrow 9e(R)$	(5.90)	5.84	0.026	87	–[i])	–	–	–[i])	–
1^1B_2	V	$1a_2 \rightarrow 2b_1$		5.91	0.016	44	5.55	0.001	21	6.17	0.010
		$+ 7e \rightarrow 8e$				23			20		
3^1A_1	V	$+ 7e \rightarrow 8e$		6.15	0	34	5.67	0	8	6.68	0
		$+ 1b_1 \rightarrow 2b_1$				11			10		
		$+ 1a_2 \rightarrow 2a_2$				–			10		
2^1B_1	R	$1a_2 \rightarrow 9b_2(R)$		6.16	0	84	–[i])	–	–	–[i])	–
2^1A_2	R	$1a_2 \rightarrow 10a_1(R)$		6.17	0	85	–[i])	–	–	–[i])	–
4^1E	R	$1a_2 \rightarrow 10e(R)$	6.40	6.38	0.059	81	–[i])	–	–	–[i])	–
3^1B_1	R	$1b_1 \rightarrow 9a_1(R)$		6.48	0	73	–[i])	–	–	–[i])	–
3^1A_2	V	$7e \rightarrow 8e$		6.80	0	81	6.25	0	2×36	6.51	0
2^1B_2	R	$1a_2 \rightarrow 3b_1(R)$		6.83	0.008	86	–[i])	–	–	–[i])	–
4^1B_1	V	$7e \rightarrow 8e$		6.84	0	81	–[i])	–	–	–[i])	–
5^1B_1	R	$1a_2 \rightarrow 10b_1(R)$		6.85	0	71	–[i])	–	–	–[i])	–
4^1A_2	R	$1b_1 \rightarrow 8b_2(R)$		6.92	0	59	–[i])	–	–	–[i])	–
		$+ 1a_2 \rightarrow 11a_1(R)$				18					–
5^1A_2	R	$1a_2 \rightarrow 11a_1(R)$		6.95	0	47	–[i])	–	–	–[i])	–
		$+ 1b_1 \rightarrow 8b_2(R)$				21					–
		$+ 1b_1 \rightarrow 9b_2(R)$				14					
5^1E	R	$1b_1 \rightarrow 9e(R)$	(7.13)	7.06	0.073	56	–[i])	–	–	–[i])	–
		$+ 1a_2 \rightarrow 11e(R)$				14					
		$+ 1b_1 \rightarrow 10e(R)$				12					
3^1B_2	V	$1a_2 \rightarrow 2b_1$	7.40	7.26	1.210	43	6.96	0.2411	49	7.70	1.0185
		$+ 7e \rightarrow 8e$				23			< 5		
6^1E	R	$1a_2 \rightarrow 10e(R)$		7.27	0.003	62	–[i])	–	–	–[i])	–
		$1b_1 \rightarrow 9e(R)$				21	–[i])	–	–	–[i])	–

[a]) At the B3LYP/6-31G* optimized geometry of **1** (see *Table 1*). [b]) V = valence, R = *Rydberg* excitation. [c]) From the spectra in *Fig. 2*. [d]) In eV, relative to the ground state. [e]) Oscillator strength for electronic transition. [f]) Contribution of excitations listed in the third column in %. [g]) From CASSCF wave function. [h]) Occupation: 27 core and inner valence shells, then $7e^2\ 1b_1^2\ 1a_2^2\ 8e^0\ 2b_1^0\ 2a_2^0\ 9a_1^0(R)\ 8b_2^0(R)\ 9e^0(R)$. [i]) *Rydberg* states not calculated by CASPT2 and TD-DFT. [k]) States dominated by doubly excited configurations cannot be calculated by the current implementation of TD-DFT.

dipole-forbidden in D_{2d} symmetry. The next two allowed transitions are calculated at only slightly higher energy than the above $1b_1 \rightarrow 8e$ excitation, but they have much smaller oscillator strengths than the latter. We, therefore, assume that they are hidden under the 5.78 eV band in the experimental spectrum. The *Rydberg* transition predicted at 5.85 eV is expected to have sharp vibrational structure and is, therefore, probably responsible for the narrow peak and a shoulder observed on the high-energy side of the 5.78 eV band in the upper spectrum of *Fig. 2*.

Table 3. *Excited Triplet States of* **1**[a])

Sym.	Type[b])	Excitation(s)[c])	Experim. energy[d])	DFT-MRCI energy	% [e])	CASPT2 energy	% [e])[f])	TD-DFT energy
1^3E	V	$1a_2 \to 8e$	2.98	2.69	66	2.86	76	2.53
		$+ 1b_1 \to 8e$			21		< 5	
1^3B_2	V	$1a_2 \to 2b_1$	4.48	4.47	41	4.64	34	4.59
		$+ 7e \to 8e$			34		40	
1^3A_1	V	$7e \to 8e$	4.52	4.69	48	4.83	46	4.82
		$+ 1b \to 2b_1$			17		21	
2^3E	V	$1b_1 \to 8e$	4.90	4.93	65	5.10	70	4.57
		$+ 1a_2 \to 8e$			23		< 5	
1^3A_2	R	$1a_2 \to 9a_1(R)$		5.09	87	$-$[g])		$-$[g])
1^3B_1	R	$1a_2 \to 8b^2(R)$		5.47	80	$-$[g])		$-$[g])
2^3B_2	V	$1a_2^2 \to 8e^2$		5.65	35	5.74	31	$-$[h])
		$+ 1b_1, 1a_2 \to 8e^2$			37		22	
		$+ 1b_1^2 \to 8e^2$			< 5		12	
3^3E	R	$1a_2 \to 9e(R)$		5.73	88	$-$[g])		$-$[g])
2^3B_1	R	$1a_2 \to 9b_2(R)$		6.02	82	$-$[g])		$-$[g])
2^3A_2	R	$1a_2 \to 10a_1 R)$		6.08	84	$-$[g])		$-$[g])
4^3E	R	$1a_2 \to 10e$		6.26	78	$-$[g])	$-$	$-$[g])
3^3A_2	V	$7e \to 8e$		6.37	48	6.12	76	6.33
		$+ 1a_2 \to 3b_1$			37		< 5	
3^3B_1	R	$1a_1 \to 9a_1(R)$		6.37	67	$-$[g])	$-$	$-$[g])

[a]) At the B3LYP/6-31G* optimized geometry of **1** (see *Table 1*). [b]) V = valence, R = *Rydberg* excitation. [c]) Occupation in the singlet ground state: 27 core and inner valence shells, then $7e^2 1b_1{}^2 1a_2^2 8^0 2b_1^0 2a_2^0 9a_1^0(R)$ $8b_2^0(R) 9e^0(R)$. [d]) From the spectrum in *Fig. 2* (lower part). [e]) Contribution of excitations listed in the third column in %. [f]) From CASSCF wavefunction. [g]) *Rydberg* states not calculated by CASPT2 and TD-DFT. [h]) States dominated by doubly excited configurations cannot be calculated by the current implementation of TD-DFT.

Following this are two valence and two *Rydberg* transitions that are all dipole-forbidden (note that one of the valence transitions leads to a doubly excited state). The next allowed transition (with a large oscillator strength for a *Rydberg* excitation) is predicted at 6.38 eV, leading to the 4^1E (3d) *Rydberg* state. The characteristic shape with three sharp peaks (0-0 transition at 6.40 eV) allows the unambiguous assignment of this band to this *Rydberg* state. Finally, the most intense band, at 7.40 eV, can be assigned to the transition to the 3^1B_2 state, which is calculated to occur at 7.28 eV with a high oscillator strength. Two narrow peaks are observed on the top, and a weak shoulder is observed on the left flank of this band. These features do not appear to form a single progression as would be expected if they were all part of the vibrational structure of the 3^1B_2 state. We, therefore, tentatively assign the shoulder at 7.13 eV (in parentheses in *Table 2*) to the 5^1E *Rydberg* state.

Table 3 shows very satisfactory agreement of experiment (*Fig. 2,b*) and theory also for the triplet states. The lowest triplet state is calculated correctly, and the existence of three triplet states in the 4 – 5 eV range is confirmed by theory. The higher-lying triplet states, including triplet *Rydberg* states, cannot be unambiguously distinguished from the singlet states in the spectrum, and we shall, therefore, not discuss their assignment here.

In view of the purpose of this investigation (*cf. Sects. 1* and *2*), a particularly significant finding is that the gap between the excitations corresponding to $1a_2 \rightarrow 8e$ and $1b_1 \rightarrow 8e$ electron promotions ($\Delta E(2,1)$ in *Sect. 2*) is *quite different* for singlet and for triplet **1** (1.32 and 1.92 eV, resp.). Note also that the calculations indicate that, in singlet **1**, the first two E states are both described well by single configurations, whereas this is not the case in triplet **1**, where the second E state is only described to about two thirds by $1b_1 \rightarrow 8e$ electron promotion, a finding which will turn out to be important in the discussion in *Sect. 4*.

Tables 2 and *3* permit a comparison of different theoretical models for **1**. The *ab-initio* CASPT2 method, which is the most demanding of the three in terms of human effort and hardware requirements, appears to be slightly more precise than DFT-MRCI for the low-lying excited states, particularly the lowest triplet, but yields predictions in slightly poorer agreement with experiment than DFT-MRCI for the higher-lying singlets. The DFT-MRCI method is sufficiently precise for unambiguous assignment in most cases and has the great advantage of treating consistently both valence and *Rydberg* states, as well as their mixing (which could also be achieved at the CASPT2 level with some effort). The DFT-MRCI method appears superior in the description of the high-lying excited states, in particular *Rydberg* states as has been impressively demonstrated in the present case on the 3d state at 6.40 eV, positively identified in the spectrum by its band shape. Finally, the TD-DFT method gives useful results for the valence states, although it is considerably less precise than the former two methods and cannot model states with predominant doubly excited character, such as the 3^1A_1 state.

3.2. *Electronic Structure of the Radical Anion* $\mathbf{1}^{\cdot-}$. It is useful to divide the electronic states of the negative ions into two categories when discussing their formation by electron impact in the gas phase (see, *e.g.*, [20] for a more thorough discussion). The first category comprises those anionic states which are formed by attaching the incident electron to the neutral target molecule such that it temporarily occupies one of its virtual MOs without changing otherwise its electronic configuration. These anionic states are called 'shape resonances' or 'one-particle resonances'. The most important decay mechanism of shape resonances is fast autodetachment of the captured electron, often accompanied by *vibrational* excitation of the target molecule. Shape resonances are, therefore, preferentially observed in the purely vibrational excitation functions, like the curve with $\Delta E = 0.6$ eV in *Fig. 3,b* (or in the transmission spectra, relying essentially on the measurement of the elastic cross section).

The second category comprises those anionic states which result from electron attachment accompanied by simultaneous electronic excitation of the target molecule. These states are called 'core excited' or 'two particles – one hole' resonances. The most important decay mechanism of such resonances is also autodetachment of the captured electron, but, in this case, the target molecule is left behind in an *electronically* excited state, generally a triplet state. Core excited-shape resonances are, therefore, preferentially observed in the excitation functions of electronically excited states, like the curves of *Fig. 3,c* and *3,d* with $\Delta E = 2.9$ eV and 5.0 eV, respectively. In analogy with the nomenclature used for positive ions when discussing UV-photoelectron and electronic-absorption spectra [21], we could also call the two types of states '*Koopmans*' and 'non-*Koopmans*' states of anions, respectively.
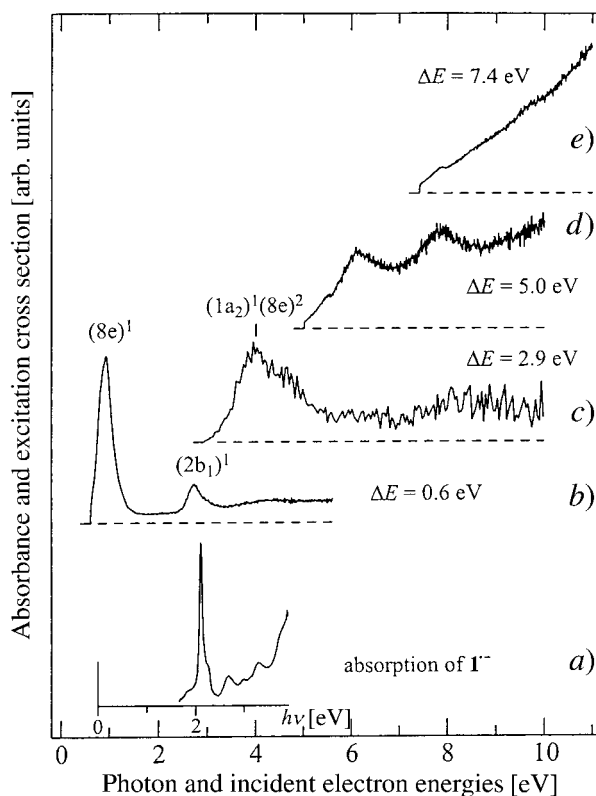
Fig. 3. *Spectra relevant to the anion* **1**·⁻: a) *electronic-absorption spectrum of the radical anion* **1**·⁻ *in an Ar matrix*; b) *electron-impact excitation functions recorded for purely vibrational excitation* ($\Delta E = 0.6$ eV; *see b*)), *excitation of two triplet states* ($\Delta E = 2.9$ *and* 5.0 eV; *see c*) *and d*)), *and for a dipole-allowed transition* ($\Delta E = 7.4$ eV; *see e*)). *The origin of the energy axis of the absorption spectrum (see a)) is placed under the center of the first shape resonance in the excitation function just above it (see b)).*

The two bands in the excitation function recorded with $\Delta E = 0.6$ eV (*Fig. 3,b*) thus indicate the presence of two shape resonances. As mentioned in the *Exper. Part*, excitation functions of purely vibrational excitation do not yield strictly vertical transitions, and bands shift slightly with the amount of vibrational excitation. *Table 4*, therefore, lists attachment energies obtained from an excitation function recorded with a very low energy loss ($\Delta E = 0.4$ eV), whereas *Fig. 3,b* shows a spectrum recorded with $\Delta E = 0.6$ eV which has otherwise better quality.

The energies of shape resonances can be approximated by an extension of *Koopmans*' theorem where SCF/6-31G virtual orbital energies are scaled with empirical parameters to obtain estimates of attachment energies (AE). Using the scaling relation of *Chen* and *Gallup* [22] (AE_i [eV] $= (\varepsilon_i[\text{eV}] - 2.33$ eV$)/1.31$), we obtain $AE_1 = 0.81$ eV and $AE_2 = 2.82$ eV. We also calculated the two attachment energies by the B3LYP method, which has been shown to yield rather accurate predictions of hydrocarbon electron affinities when the basis set comprises diffuse functions [23]. Using the 6-31 + G* basis set, we obtained a value of 0.73 eV for the

Table 4. *Experimental and Calculated Electron-Attachment Energies* (AE) *in eV*

Experimental AE (± 0.2 eV)	Calculated AE		Anion electron configuration
	Koopmans[b])	B3LYP/6-31 + G*[c])	
0.8[a])	0.81	0.73	... $(1a_2)^2 (8e)^1$
2.7[a])	2.82	–	... $(1a_2)^2 (2b_1)^1$
4.0	–	–	... $(1a_2)^1 (8e)^2$
6.1	–	–	core excited
7.8	–	–	core excited

[a]) From a vibrational excitation function recorded at a 0.4 eV energy loss. [b]) Derived from HF/6-31G virtual orbital energies with the scaling relation described in the text. [c]) Difference between the total energy of the anion and the neutral molecule.

vertical electron affinity of **1**, again in good agreement with experiment and with the above *Koopmans*-type calculations. Taken together, these calculations leave no doubt with regard to the assignment of the shape resonances in *Fig. 3,b* as electron captures into the 8e and the $2b_1$ orbitals, respectively.

The excitation function recorded with $\Delta E = 2.9$ eV (excitation to the lowest triplet state) indicates a core-excited resonance at 4.0 eV (*Fig. 3,c*). The lowest core-excited resonance which can decay into the HOMO → LUMO excited triplet state by the ejection of one electron (without simultaneously changing the remaining electron configuration) has the occupation pattern ...$(1a_2)^1(8e)^2$, and, therefore, we assign the 4 eV band to this resonance. Relative to the ground state of $\mathbf{1}^{\cdot-}$, which lies at 0.8 eV, this resonance is formally attained by $1a_2 \rightarrow 8e$ electron promotion, *i.e.*, it corresponds to the HOMO → LUMO $(1 \rightarrow -1)$ excitation in **1**. Hence this excitation is associated with an energy of $4.0 - 0.8 = 3.2$ eV, a feature that we wish to retain for the purpose of the discussion in *Sect. 4*.

The excitation function recorded with $\Delta E = 5.0$ eV (*Fig. 3,d*) shows two bands corresponding to higher-lying core-excited resonances, but we lack the theoretical means to propose a well founded assignment for them. Nevertheless, the excitation function is useful, since the very presence confirms the existence of a triplet state at 5 eV. Finally, the nearly linear excitation function recorded with $\Delta E = 7.4$ eV (*Fig. 3,e*) is characteristic for a dipole-allowed transition, in accord with the assignment of the 7.40 eV state given in *Table 2*.

As a complement to the above experiment, we explored the excited-state structure of $\mathbf{1}^{\cdot-}$ by generating this species radiolytically in a low-temperature matrix and recording its electronic-absorption (EA) spectrum. The curve of *Fig. 3,a*, shows the spectrum of a 0.01M solution of **1** in methyltetrahydrofuran (MeTHF) after 0.5 Mrad ^{60}Co γ-irradiation at 77 K. Its main feature is a sharp band at 16950 cm^{-1} that is accompanied by a high-energy shoulder. As we will show below, this band may be assigned to excitation from the singly occupied 8e to the $2b_1$ MO of $\mathbf{1}^{\cdot-}$. Therefore, the excitation energy (2.10 eV) should be comparable to the *difference* in energies of the two shape resonances seen in *Fig. 3,b* (1.9 ± 0.2 eV). This is the case, except for a shift of *ca.* 0.2 eV between the two experiments which is, however, not unexpected for two reasons: *a*) The electron attachment experiment refers to vertical transitions at the geometry of the neutral molecule. The matrix photoabsorption experiment refers to

vertical transitions at the (relaxed) geometry of the electronic ground state of the anion. The transition energies can, therefore, not be expected to be exactly equal. It will be argued below that the geometry relaxation of the anion corresponds primarily to a *Jahn-Teller* (*JT*) distortion, since the extra electron is accommodated in a degenerate MO. *b*) The environment will exert a strong influence on the anion, which will be different for the ground and the various excited states of $\mathbf{1}^{\cdot-}$, leading to shifts in the energies of the excited states on going from the gas phase to MeTHF.

Let us begin by addressing the first of the above issues: According to group theory, for a system of D_{2d} symmetry, *JT* distortion will occur along b_1 and b_2 modes leading to structures of D_2 or D_{2v} symmetry, respectively. In the absence of second-order effects, one of the two structures will be a minimum and the other a transition state on the 'moat' that surrounds the conical intersection of the two states in D_{2d}.

We attempted to gain more insight into the nature of the *JT* distortion by carrying out quantum-chemical calculations on the radical anion. Such calculations are, strictly speaking, not applicable to the radical anion in the gas phase, because it lies in the energy continuum of a free electron and the ground electronic state of the neutral molecule, *i.e.*, the variational principle does not apply. However, the calculations may nevertheless yield useful information when the additional electron is held in the vicinity of the molecule by choosing basis-set functions of finite spatial extent which effectively prevent the attached electron to escape into the continuum. The calculations may be fully justified for the condensed phase, where the ground electronic state of the anion is probably stabilized towards autodetachment by solvation.

The above expectation of a *JT* distortion is confirmed by geometry optimizations carried out on $\mathbf{1}^{\cdot-}$ by the B3LYP method (*cf. Table 1*): relaxation in D_2 results in a change of the dihedral angle θ between the cyclopentadiene moieties from 90° to 78.7° and leads to a structure that represents a minimum on the potential-energy surface. Conversely, optimization in C_{2v} results in a structure which reveals itself as a saddle point, thus serving as a transition state on the *JT* moat for the interconversion of equivalent D_2 states. Note that in this C_{2v} species, spin and charge are largely localized in one of the diene moieties. This makes sense in view of the fact that, to pass from one D_2 structure to the other ($^2B_2$ to $^2B_3$ conversion in *Fig. 4*), the phases of the π MOs in one of the diene moieties must *change*, which they can only do if the coefficients of the p-AOs vanish at some point.

As a result of the attachment of an electron in a π^* MO of $\mathbf{1}$, the C−C bond-length alternation in the diene moiety decreases from 0.13 Å in the neutral to 0.07 Å in the (delocalized) D_2 state of the radical anion, whereas the other structural parameters are only slightly affected (see *Table 1*). As a consequence of the localization of spin and charge at the C_{2v} geometry, the C−C bond length alternation is *inverted* in one of the rings (-0.013 Å), whereas it remains at $+0.13$ Å in the other. The energy difference between the two structures is rather small (2.3 kcal/mol at the B3LYP/G-31G* level), and so is the energy gained by *JT* distortion and relaxation from the neutral geometry (4.0 kcal/mol by B3LYP/6-31G*, 5.7 kcal/mol by CASPT2), *i.e.* the potential-energy surface is quite flat in the vicinity of the stationary points. Nevertheless, we assume that the absorption spectrum of $\mathbf{1}^{\cdot-}$ was obtained at its D_2 equilibrium geometry, in contrast to the above-described electron-scattering experiments which yielded *vertical* anion
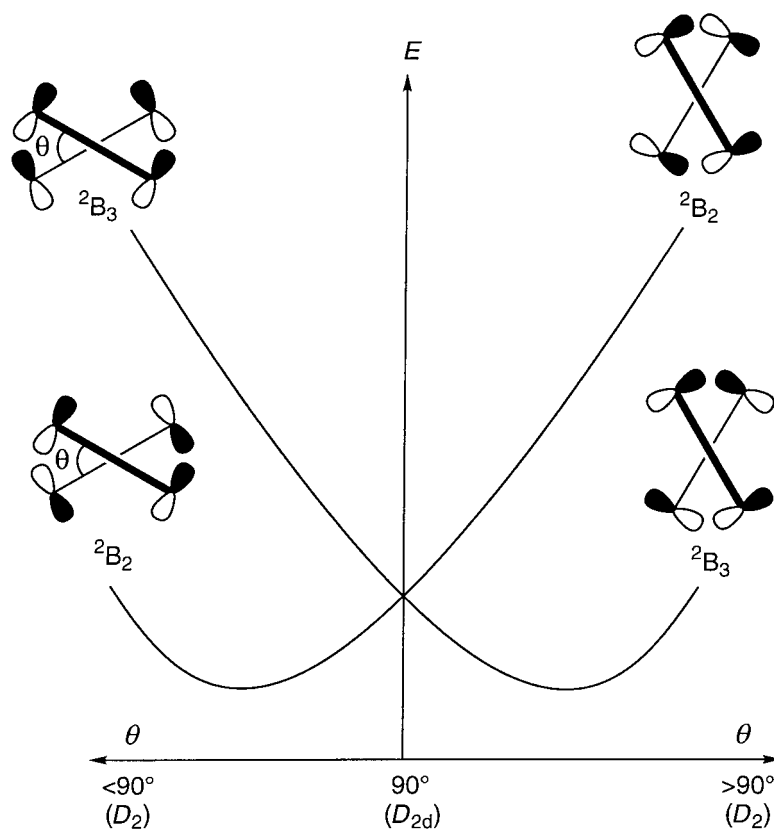
Fig. 4. *Schematic potential-energy surfaces for the* D_{2d} *to* D_2 Jahn-Teller *distortion of* **1**$^{\cdot-}$. Note that the two components of the degenerate state in D_{2d} are stabilized or destabilized, respectively, by bonding or antibonding spiroconjugative interaction of the component π MOs, shown in a head-on view.

resonances at the neutral geometry. This geometry change affects, of course, the position of the anion's spectral bands.

To assess the influence of *JT* distortion on the energies of the excited electronic states of **1**$^{\cdot-}$, we attempted CASPT2 calculations on the anion. However, this venture met with intriguing difficulties related to the above-mentioned fact that it is principally impossible to treat states imbedded in the autodetachment continuum by variational methods. Admitting the MOs shown in *Fig. 1* in the active space resulted in a set of reasonable CASSCF wave functions. However, in the ensuing CASPT2 calculations, it became evident that excitations into higher-lying π MOs, formed primarily by linear combinations of the outer, diffuse components of the split valence basis set, attain so much weight that their contribution cannot be treated anymore by perturbation theory. These problems arise as a consequence of a (failed) attempt of the method to represent continuum states. In addition, excitations into low-lying σ^* MOs were found to give rise to excited states in the region covered by the experimental spectra. Unfortunately, admitting all these virtual MOs into the active space led to an increase in the number of configurations that could no longer be handled computationally.

Therefore, we limited ourselves to a treatment of the first excited state (1^2B_1 in D_{2d}, 1^2A in D_2 symmetry), *i.e.*, the state that gives rise to the first band at 2.1 eV in the electronic-absorption spectrum and to the second shape resonance at 2.68 eV seen in *Fig. 3,b*. CASSCF and TD-DFT calculations show that this state is well described by a single configuration, formed by attachment of an electron in the second lowest π^* MO of **1** (see above). Therefore, and because it is of different symmetry from the ground state, it is amenable to single-determinant calculations.

Thus, we carried out B3LYP calculations on both states of **1**$^{\cdot-}$. At the neutral geometry, the 1^2B_1 state lies 2.12 eV above the ^2E ground state[2]), in reasonable agreement with experiment if the calculation is carried out with the 6-31G* basis set. However, on addition of a set of diffuse functions (6-31 + G*), which had proven necessary to get a good estimate of the electron affinity (see above), the energy difference falls to 0.44 eV because the diffuse functions gain much more importance in the excited state whose coupling to the continuum is stronger. More importantly, on relaxation of the geometry to the D_2 equilibrium structure of ground state **1**$^{\cdot-}$, the excited-state energy *increases* by 0.33 eV (0.36 eV with 6-31 + G*) relative to the ground state.

From the above result, we conclude that the observed 0.2-eV shift of the energy difference between the ground state and the first excited state as probed by the two experiments is mainly due to the change in *geometry*. If the change in the *environment* has any effect at all, it is probably in the opposite direction, *i.e.* solvation stabilizes the excited state more than the ground state.

3.3. *Electronic and Vibrational Structure of the Radical Cation* **1**$^{\cdot+}$. *Fig. 5* shows the electronic-absorption spectrum observed after X-irradiation of **1** embedded in a CH_2Cl_2-doped Ar matrix. The most notable feature of this spectrum is the highly structured NIR band which, according to the calculations listed in *Table 5*, corresponds to promotion of an electron from the spiro-bonding ($1b_1$) to the spiro-antibonding combination of diene MOs ($1a_2$), *i.e.* to $1^2A_2 \rightarrow 1^2B_1$ excitation. The same excited state is attained by ejection of an electron from the $1b_1$ MO of **1**, thus giving rise to the second band in the PE spectrum. Indeed, the energy of the vertical transition (1.29 eV) matches very well the energy difference between the first and second PE band (1.23 eV) [6], thus lending additional support to the above assignment.

Apart from this interesting band, to which we shall return below, the spectrum shows a few additional nondescript absorptions that would be difficult to assign to any of the excited states predicted by the calculations listed in *Table 5*, were it not for the fact that **1**$^{\cdot+}$ can be converted to the radical cation of indene, **2**$^{\cdot+}$, by irradiation at 450 nm (dashed trace in *Fig. 5*), presumably *via* a [1,5] vinyl shift.

This conversion, which parallels the thermal [7] and photochemical[3]) decay of **1**, is accompanied by a decrease of the absorption at 350 – 500 nm which indicates the presence of a broad band of **1**$^{\cdot+}$ peaking in this region (*ca.* 2.8 eV). This is in accord with the predicted transition to an ^2E state (electron promotion from the 7e to the $1a_2$ MO of **1**$^{\cdot+}$ or ejection of an electron from the 7e MO of **1**) that carries a significant

---

[2]) Due to problems in SCF calculations of degenerate states, both states were calculated at slightly distorted geometries of D_2 symmetry.
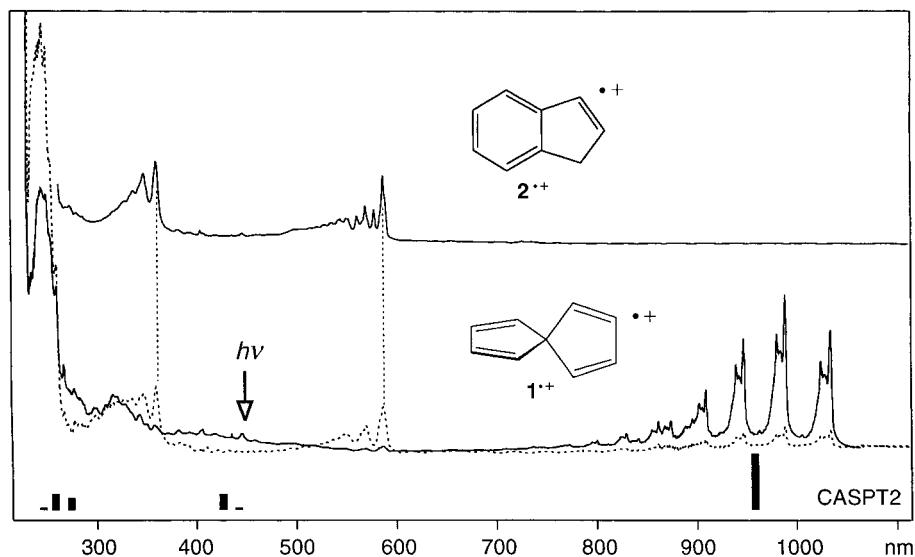
[3]) See footnote 14 and remark on p. 7663 of [6].

Fig. 5. *Electronic-absorption* (EA) *spectrum of* **1** *after ionization in Ar at 12 K* (solid line, bottom) *and after subsequent bleaching by irradiation through a 450-nm interference filter* (dashed line, bottom), *as well as the spectrum obtained by ionization of indene* **2** *in Ar under the same conditions* (top). CASPT2 *predictions of excited-state energies and oscillator strengths for* **1**[.+] (cf. *Table 5*) *are indicated by vertical bars.*

Table 5. *Excited Doublet States of* **1**[.+]

Sym.	Excitation(s)[c) ΔE[d)	Exper.[a) ΔE[d)[e)	CASPT2[b) ΔE[d)[e)	f[f)	TD-DFT ΔE[d)[e)	f[f)
1^2A_2	83% ground config.[g)	(0)	(0)	–	(0)	
1^2B_1	80% $1b_1 \rightarrow 1a_2$	1.27	1.29	0.0996	1.62	0.0031
1^2E	38% $1a_2 \rightarrow 8e$ + 33% $1b_1 \rightarrow 8e$	–	2.80	0.0020	2.89	$< 10^{-4}$
2^2E	71% $7e \rightarrow 1a_2$	(2.56)[h)	2.90	0.0282	3.13	0.0018
3^2E	28% $1a_2 \rightarrow 8e$ + 23% $1b_1 \rightarrow 8e$ + 19% $6e \rightarrow 1a_2$	> 4.5	4.52	0.0213	4.19	0.0009
4^2E	28% $1a_2 \rightarrow 2b_1$ + 21% $7e \rightarrow 8e$	> 4.5	4.81	0.0270	4.99	0.0135

[a) Vertical transitions from electronic absorption spectrum in Ar, *Fig. 5,b*. [b) Based on a (13,12) CASSCF calculation (1 occupied plus 1 virtual MO of a_1, a_2, and b_1 symmetry each, and $4+2$ MOs of e symmetry). [c) Leading contributions, from CASSCF wavefunction, in terms of the MOs depicted in *Fig. 1*. [d) Energies relative to ground state in eV. [e) At the B3LYP/6-31G* optimized geometry of the ground state (cf. *Table 1*). [f) Oscillator strength for electronic transition. [g) Occupation: 27 core and inner valence shells, then $7e^2 1b_1^2 1a_2^1 8e^0 2b_1^0 2a_2^0$. [h) $I_3 - I_1$ energy difference from the photoelectron spectrum [6]. In the absorption spectrum of **1**[.+], a broad band appears around 2.8 eV.

oscillator strength. Indeed, the position of this state matches quite well the energy difference $I_3 - I_1 = 2.56$ eV from the photoelectron spectrum [6], the small discrepancy being probably due to the change in geometry on ionization. Another much weaker

transition to a ^2E state that arises in part by $1a_2 \rightarrow 8e$ (HOMO $\rightarrow$ LUMO) excitation probably does not manifest itself in the spectrum due to its expected low oscillator strength (*cf. Table 5*). Conversely, the hump at *ca.* 320 nm that arose on ionization of **1** must be attributed to a by-product because it changes barely in intensity on bleaching of **1·⁺**, in spite of the fact that **2·⁺** shows no absorption band in this region. Higher-lying excited states predicted at 4.5 – 5 eV are masked by absorptions of neutral **1**, and of **2·⁺** which is already present in small concentration after ionization of **1**.

Returning to the interesting first absorption band of **1·⁺**, which is shown on an expanded energy scale in *Fig. 6*, we note that the vibronic structure of this band is dominated by a long progression of 442 ± 1 cm⁻¹. Since the π-bond orders *within* the two diene moieties undergo only very small changes in the course of the $1b_1 \rightarrow 1a_2$ electron promotion, no significant structural changes are expected to occur within the two diene moieties. In contrast, the fact that the promotion occurs from the spiro-bonding to the spiro-antibonding combination of diene MOs is expected to lead to an increase in the distance *between* the diene moieties.
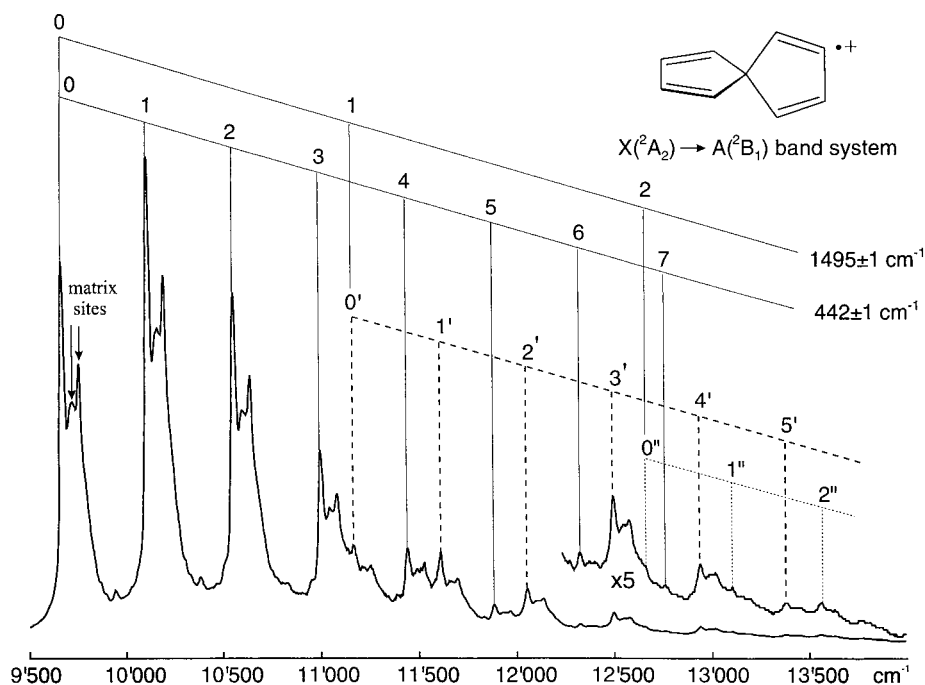

Fig. 6. *Expanded view of the first EA band of* **1·⁺** *on an energy scale* (see text)

Indeed, geometry optimization of the 1^2B_1 state of **1·⁺** led to a potential-energy minimum which differs from that of the 1^2A_2 ground state mainly by the distance between the diene moieties (see *Table 1*, structural parameters *a* and *d*). In *Fig. 7*, the distortion suffered by **1·⁺** on $1^2A_2 \rightarrow 1^2B_1$ excitation is shown in the form of atomic-displacement vectors (relative to the central atom being the center of gravity of the molecule). A vibrational calculation at the 1^2B_1 equilibrium structure revealed a totally

symmetric normal mode of 443 cm^{-1} (right side of *Fig. 7*), which nearly coincides with the above displacements. Hence it comes at no surprise that this normal mode is mainly excited in the course of the $1^2A_2 \rightarrow 1^2B_1$ excitation. The excellent match between the calculated and the observed frequencies of this vibration is noteworthy, though probably fortuitous.
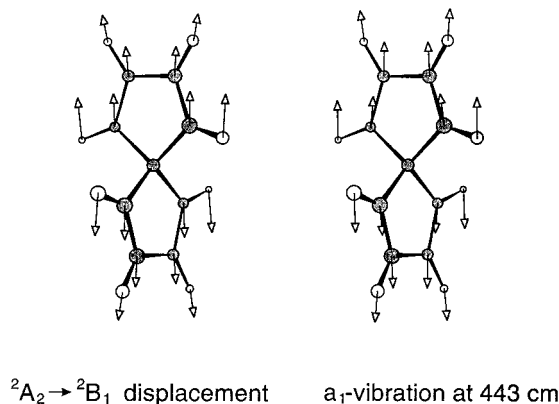

$^2A_2 \rightarrow {}^2B_1$ displacement a_1-vibration at 443 cm

Fig. 7. *Vectorial representation of the displacements undergone by* **1**·⁺ *on $1^2A_2 \rightarrow 1^2B_1$ excitation, and of the a_1 vibration at 443 cm^{-1} in the 1^2B_1 excited state*

Each member of the 442 cm^{-1} progression is further split into a triplet of (resolved) bands separated by 50 ± 3 and $88 \pm 3 \text{ cm}^{-1}$, respectively. Since no normal modes of such low frequency exist in the 1^2B_1 state of **1**·⁺, we propose to attribute this fine structure to shifts that are caused by the accommodation of **1**·⁺ in differently shaped cavities of the Ar matrix ('site splittings'). This assignment could potentially be substantiated by site-selective photolyses, such as they were effected, *e.g.*, in the case of the radical cation of octatetraene [24]. However, this is not straightforward in the present case because the required highly monochromatic NIR light sources are not readily available.

Finally we wish to note that the *Franck-Condon* envelope between 9500 and 11500 cm^{-1} repeats itself with a new origin at 11170 cm^{-1} (dashed lines, primed numbers in *Fig. 6*). In a highly expanded spectrum, a further repetition can be discerned with an origin at 12665 cm^{-1} (doubly primed numbers). These repetitions correspond to excitation of a normal mode of $1495 \pm 1 \text{ cm}^{-1}$. Indeed, the B3LYP calculations predict totally symmetric vibrations in this region, and the one at 1566 cm^{-1}, which corresponds to a shortening of the double and a lengthening of the essential single diene bonds, would seem to fit quite well in view of the fact that the π-bond orders increase slightly along the former and decrease along the latter on $1b_1 \rightarrow 1a_2$ electron promotion (*cf.* MOs in *Fig. 1*).

We also followed the ionization of **1** and the subsequent bleaching of its radical cation to **2**·⁺ by vibrational spectroscopy, as illustrated in *Fig. 8*. There, the peaks which decrease on X-irradiation (solid line) are those of neutral **1**, and they are seen to correlate very well with the ones predicted by a harmonic B3LYP force field shown at the bottom of *Fig. 8*. The peaks, which rise on ionization (solid line) and decrease on subsequent 450 nm bleaching (dashed line), can be assigned to **1**·⁺. In this case, the

correlation with the predictions from the calculated force field is a bit less impressive, but nevertheless all important vibrational bands of $\mathbf{1}^{\cdot+}$ can be clearly discerned in the spectrum. Finally, the bands marked with asterisks in the dashed line correspond to the strongest peaks in the IR spectrum of $\mathbf{2}^{\cdot+}$, which requires, however, no additional identification due to its clear presence in the optical spectra.
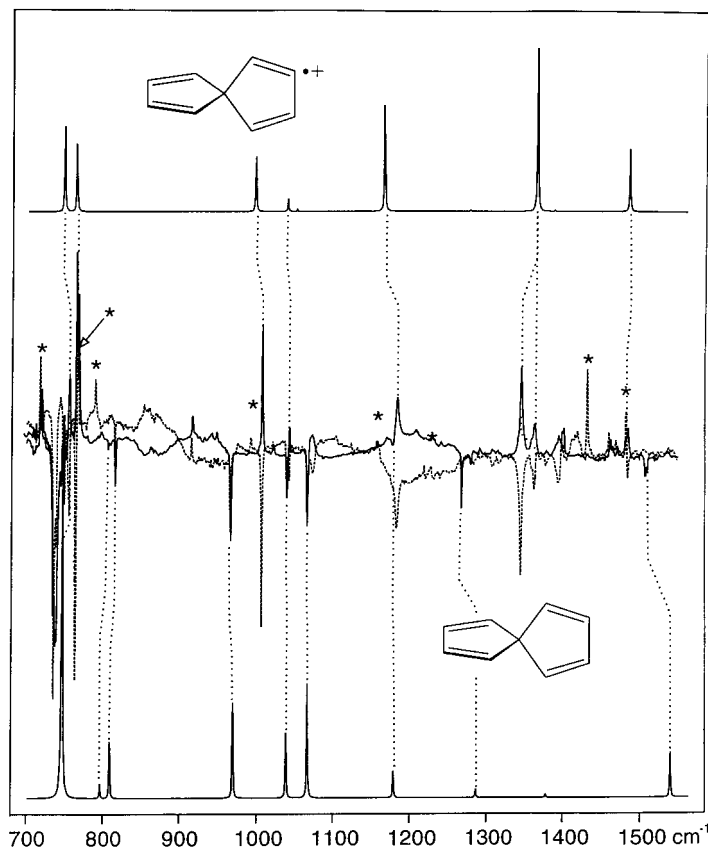

Fig. 8. *IR Difference spectra for the ionization of* $\mathbf{1}$ (solid line) *and for the subsequent bleaching of* $\mathbf{1}^{\cdot+}$ (dashed line). The bottom and the top traces represent the IR spectrum of $\mathbf{1}$ and $\mathbf{1}^{\cdot+}$, respectively, calculated by the B3LYP/6-31G* method. The bands marked with asterisks in the dashed line correspond to the strongest peaks in the IR spectrum of $\mathbf{2}^{\cdot+}$.

In *Table 6*, we list some selected vibrations of $\mathbf{1}$ and $\mathbf{1}^{\cdot+}$ as they are predicted by B3LYP and observed in the IR spectra (the full list is available in the *Supporting Information*). The modes listed in *Table 6* were found to correlate quite well between $\mathbf{1}$ and $\mathbf{1}^{\cdot+}$ by visual inspection, a feature which is, however, not uniformly preserved, especially for the low-frequency vibrations where the normal modes differ quite substantially in the two species.

As expected from the nodal properties of the a_2 HOMO from which ionization occurs (*cf. Fig. 1*), all vibrations that involve C=C stretching decrease in energy on ionization because the π-bond orders along these bonds decrease. Unfortunately, the

Table 6. *Selected Vibrations of* **1** *and* **1**[·+]

Sym.	Description[a])	**1**		**1**[·+]	
		calculated[b])	observed[c])	calculated[b])	observed[c])
e	asym. $\tilde{\nu}$(C=C)	1657 (≈ 0)	–	1544 (93)	1485
a_1	sym. $\tilde{\nu}$(C=C)	1591 (0)	–	1508 (0)	–
b_2	asym. $\tilde{\nu}$(C=C)	1572 (8)	1508	1419 (270)	≈ 1352[d])
b_2	ρ(C–H)	1204 (5)	1177	1212 (160)	1183
e	ρ(C–H)	1313 (2)	1266	1328 (1)	–
e	ρ(C–H)	1090 (20)	1065	1093 (2)	–
b_2	ρ(C–H)	1061 (11)	1039	1080 (17)	1042
a_1	$\tilde{\nu}$(C–C)[e])$+\rho$(C–H)	1009 (0)	–	1068 (0)	–
b_2	$\tilde{\nu}$(C–C)[e])$+\rho$(C–H)	991 (16)	966	1038 (77)	1006
b_2	ring deformation	827 (10)	815	795 (97)	764
e	ring deformation	814 (2)	805	819 (≈ 0)	–
e	ω(C–H)	764 (120)	736	779 (62)	755

[a]) $\tilde{\nu}$ Stretch; ρ, rock; ω, wag. [b]) From B3LYP/6-31G*, all vibrations scaled by 0.97; intensities in km/mol in parentheses. [c]) See IR spectra in *Fig. 8*. [d]) Weighted average between the two bands at 1346 and 1363 cm^{-1}; see text for explanation. [e]) sp^2-sp^2 essential single bonds.

only one of these modes that could be observed is that of b_2 symmetry, which falls from 1508 cm^{-1} in **1** to *ca.* 1350 cm^{-1} in **1**[·+] (the corresponding IR peak is split into two components that arise presumably by a *Fermi* resonance with an IR-forbidden transition or an overtone or combination band, the weighted average of the two frequencies is listed in *Table 6*). A surprising feature here is the strong rise in intensity of the corresponding IR transition on ionization, a feature for which we have no explanation.

In contrast, the modes that involve a stretching of the central C(sp^2)–C(sp^2) bonds, only one of which was observed, increase in energy on ionization, again in accord with the fact that the π-bond orders along these bonds increase on ionization. Finally, modes which involve mainly C–H rocking or wagging motions undergo much smaller shifts on ionization. In fact, most of them increase slightly in energy, presumably because the entire C-frame becomes a bit stiffer through the rise in double-bond character of the central C(sp^2)–C(sp^2) bonds.

Surely the agreement between theory and experiment, notably for **1**[·+], could be improved by a judicious scaling of the B3LYP force field as it had been achieved previously for the related molecule, cyclopentadiene [25]. However, we did not expect to gain any additional insight from that, so we refrained from embarking on this exercise in the present case.

4. Corollaries. – As mentioned in *Sects. 1* and *2*, the purpose of the present work was to examine *a*) whether the simple relationship $\Delta^1 E(2,1) = \Delta I(2,1)$ that had been found and rationalized by *Heilbronner* and co-workers for **1** extends also to the corresponding triplet state, *i.e.*, $\Delta^3 E(2,1)) = \Delta I(2,1)$, and *b*) if *a*) holds, whether the $1 \rightarrow -1$ excitations in the singlet, the triplet, and the doublet manifold of states obey the SDT rule, *i.e.*, $^2 E(1 \rightarrow -1) = [^1 E(1 \rightarrow -1) \cdot ^3 E(1 \rightarrow -1)]^{1/2}$.

A pivotal prerequisite for all of the above simple relationships to hold is that all involved electronic states can be described essentially by single MO configurations. The

results of our calculations show that this condition is fulfilled quite well by the first two excited singlet states (1^1E and 2^1E in *Table 2*) as well as for the first excited doublet state of $\mathbf{1}^{\cdot+}$ (1^2B_1 in *Table 5*). In retrospect, it is exactly this feature which allowed *Heilbronner* and co-workers to positively rationalize the observed relation $\Delta^1E(2,1) = \Delta I(2,1)$!

However, the EEL spectrum of **1** in *Fig. 2* demonstrates that the triplet states do not conform with expectations based on a single-configuration model, in that $\Delta^3E(2,1) = 1.92$ eV is nearly 50% higher than $\Delta^1E(2,1) = 1.32$ eV (instead of being of equal magnitude). The reason for this discrepancy becomes evident from *Table 3* which shows that the first two triplet configurations undergo significant interaction (CI), in contrast to the corresponding singlet configurations. To understand this outcome, we carried out some INDO/S-CI model calculations at the B3LYP/6-31G* optimized geometry of **1**.

In conformity with the findings of *Heilbronner* and co-workers, $\Delta E(2,1)$ of the singlet and triplet *configurations* is indeed very similar (1.98 and 1.78 eV, resp.) and close to $\Delta I(2,1)$ (1.85 eV). However, whereas $\Delta E(2,1)$ hardly changes on going *via* CI to final singlet *states* ($\Delta^1E(2,1) = 2.00$ eV), it increases to $\Delta^3E(2,1) = 3.7$ eV in the triplet manifold[4]). This must be due to significantly different off-diagonal CI-matrix elements within the two multiplicity manifolds.

If we define the two electron-repulsion integrals by *Eqns. 6* and *7* (MO numbering as in *Fig. 1*), then the off-diagonal singlet and triplet CI-matrix elements can be expressed by *Eqns. 8* and *9*, respectively.

$$A = \langle \Psi_1(1)\Psi_2(1) \,|\, e^2/r_{12} \,|\, \Psi_{-1}(2)\Psi_{-1}(2)\rangle \tag{6}$$

$$B = \langle \Psi_1(1)\Psi_{-1}(1) \,|\, e^2/r_{12} \,|\, \Psi_2(2)\Psi_{-1}(2)\rangle \tag{7}$$

$$^1CI = 2B - A \tag{8}$$

$$^3CI = -A \tag{9}$$

From INDO/S-CI, we obtain $A = -1.42$ eV and $B = -0.77$ eV. Because B is about half as large as A, the two nearly cancel in ^1CI which is therefore only -0.12 eV. Hence, the virtual absence of CI for the first two excited singlet states of **1** is due to a fortuitous cancellation of terms in the off-diagonal CI-matrix element, which makes it possible for the simple relationship $\Delta^1E(2,1) = \Delta I(2,1)$ to be fulfilled in practice. In contrast, the corresponding matrix element in the triplet case is significantly different from zero, which is why $\Delta^3E(2,1)$ does not conform with expectations based on a single configuration model for **1**.

The occurrence of significant CI in $^3\mathbf{1}$ deprives of course also the SDT rule of its premises. Furthermore, our calculations on $\mathbf{1}^{\cdot+}$ (*Table 5*) show that CI is also important in the doublet manifold. Actually, the $1 \to -1$ excited configuration is distributed evenly over several excited states such that no single electron promotion can be

---

[4]) The *absolute* values of these numbers are in poor agreement with experiment, but the trends are in accord with observations and with the high-level calculations shown in *Tables 1* and *2*.

associated with this excitation. In addition, these transitions have all very small oscillator strengths so that they cannot be discerned in the experimental spectrum of $\mathbf{1}^{\cdot+}$. The situation is a bit better in $\mathbf{1}^{\cdot-}$, where a resonance that lies 3.2 eV above the ground state was identified with the $1 \rightarrow -1$ excited state. This energy lies, indeed, between the corresponding excitations in $^1\mathbf{1}$ (4.46 eV) and $^3\mathbf{1}$ (2.98 eV), but, in view of the CI that prevails in $^3\mathbf{1}$ (and presumably also in $\mathbf{1}^{\cdot-}$), no quantitative conclusions can be drawn with regard to the validity of the SDT rule in this case.

5. Conclusion. – By measuring electron-energy-loss spectra, we have been able to determine the triplet energies of the title compound $\mathbf{1}$. Thereby, we found that the gap between the first two triplet states is *ca.* 50% larger than between the corresponding singlet states, which makes the elegant treatment, proposed 25 years ago by *Heilbronner* and co-workers, inappropriate for the triplet states. We show that the reason for this discrepancy lies in the occurrence of strong CI for the first two triplet states which, however, is nearly absent for the corresponding singlet states.

In addition, we measured the electronic-absorption spectra of $\mathbf{1}^{\cdot+}$ and $\mathbf{1}^{\cdot-}$ in low-temperature matrices, as well as excitation functions that reveal different resonances of gas phase $\mathbf{1}^{\cdot-}$. This allowed us to gain insight into the first few excited states of the radical ions. In the case of $\mathbf{1}^{\cdot+}$, the most interesting feature is a highly structured near-IR absorption band, which coincides with the second band in the photoelectron spectrum. The most prominent progression in this band is explained in terms of a vibration that is preferentially excited on relaxation of $\mathbf{1}^{\cdot+}$ in its first excited state from the ground-state geometry. On near-UV irradiation, $\mathbf{1}^{\cdot+}$ was found to decay to the radical cation $\mathbf{2}^{\cdot+}$ of indene.

Experimental Part

1. *Synthesis.* Spiro[4.4]nona-1,3,6,8-tetraene (**1**) was prepared as previously reported [4].

2. *Gas-Phase Experiments.* The trochoidal electron spectrometer used in the present work has been described in detail previously [20][26][27]. It uses magnetic collimation of the electron beams, trochoidal monochromators as electron-energy filters, and a collision chamber with small apertures for the incident and scattered electron beams. The experiment involves intercepting the sample vapor at low pressure (*ca.* 10^{-4} mbar) with a beam of electrons of varying incident energy E_i and detecting electrons scattered at a fixed residual energy E_r. The incident electrons can excite the target molecules, thereby loosing an amount of kinetic energy $\Delta E = E_i - E_r$ equal to the excitation energy. A spectrum of excited states is obtained by plotting the scattered-electron current against the electron-energy loss ΔE.

The residual energy of 20 eV is sufficiently high to cause the spectra recorded at this energy to be dominated by dipole-allowed transitions and band intensities indicative of the dipole oscillator strengths. (The electron energy is not high enough for the dipole limit to be reached quantitatively, the relative intensities of the bands may differ from the dipole intensities, and dipole-forbidden singlet transitions may also appear in the spectra. A qualitative comparison of band intensities with calculated and measured oscillator strengths is, however, meaningful). Triplet bands appear in the spectra recorded with low residual energies. The cross sections for excitation of the triplet states are not forward peaked, but more isotropic with respect to scattering. The capacity of the present instrument to detect the backward scattered electrons [20][27] is thus essential for the detection of triplet states.

Electron-impact spectroscopy can determine the energies of the ground and the excited states of the radical anion by detecting a (temporary) attachment of the incident electrons to form short-lived anions (alternately called 'resonances'). The attachment energies are generally measured by electron-transmission spectroscopy

(ETS). ETS could not be applied to **1**, however, because it requires more sample than we had available (*ca.* 20 mg) and a vapor pressure higher than we could attain (the sample had to be kept at $-20°$ during the measurement to prevent polymerization). We, therefore, chose the essentially equivalent method of measuring the excitation functions of vibrational excitation.

Vibrational excitation by electron impact is generally mediated by resonances (*i.e.* various states of the temporary anion), which consequently appear in the excitation functions as bands. This method has the advantages of lower requirements on the amount and vapor pressure of the sample, and of being (in contrast to ETS) a 'zero background' technique. The attachment energies determined in this way are generally slightly (*ca.* 0.1–0.2 eV) higher than those determined by ETS (a consequence of *Franck-Condon* factors associated with the detection of vibrationally excited molecules), but this effect can be minimized by measuring excitation functions for lower-lying vibrationally excited states.

3. *Condensed-Phase Experiments*. The radical cations of **1** and indene were generated by X-irradiation of samples of the neutral precursors isolated in Ar at 12 K in the presence of an equimolar amount of CH_2Cl_2 as an electron scavenger, with the techniques described previously [28]. Electronic absorption spectra were taken between 200 and 1200 nm with a *Perkin-Elmer Lambda-19* instrument, whereas IR spectra were obtained on a *Bomem-DA3* interferometer (1-cm^{-1} resolution) equipped with an *MCT* detector (500–4000 cm^{-1}). The photolysis of **1**$^{·+}$ was effected by a 1-kW Ar plasma discharge lamp through a 450 nm interference filter.

The radical anion of **1** was prepared by ^{60}Co γ-irradiation (0.5 MRad) of a frozen 10^{-2} M soln. of **1** in dry degassed methyltetrahydrofuran (MeTHF), a solvent that forms a transparent glass at 77 K and serves as an efficient hole trap [29].

4. *Quantum-Chemical Calculations*. The geometries of all species were optimized by the B3LYP density functional method [30][31] as implemented in the Gaussian 98 suite of programs [32][33], with the 6-31G* basis set (*cf. Table 1*). Relative energies and vibrational spectra were calculated at the same level. Full sets of cartesian coordinates and absolute energies (including thermal corrections where available) are given in the *Supporting Information*.

Excited-state calculations were carried out at B3LYP/6-31G* equilibrium geometries of the neutral or the radical cations, respectively, by three different procedures.

One of them is the CASSCF/CASPT2 procedure [34] as implemented in the MOLCAS program [35] using the [C,N,O]3s2p1d/[H]2s ANO basis set [36]. The active spaces were chosen such that the weight of the zero-order CASSCF in the CASPT2 wave function exceeded 66% for all states. The resulting active spaces are described in the *Footnotes* to *Tables 1*, *3*, and *5*. To ensure orthogonality, the CASSCF wave functions were averaged over all excited states of the same symmetry. Transition moments were calculated with the RASSI program in the velocity representation using CASPT2 energy differences in the denominator.

In the case of the singlet and triplet excited states of neutral **1**, DFT-MRCI calculations [37] were performed with the TURBOMOLE suite of programs [38][39]. These calculations gave insight both into valence and *Rydberg* states. Valence triple-ζ Gaussian AO basis sets augmented with polarization functions on all atoms ([5s3p1d]/[3s1p] [40]) were used. In the DFT-MRCI method, the BHLYP functional [41] was used to ensure a proper description of the asymptotic form of the potential far away from the nuclei, which is important for a description of *Rydberg* states. In these calculations, the AO basis was augmented by one set of diffuse spd functions ($\alpha = 0.04$) on each C-atom. With an energy cutoff value of 1.0 hartree, *ca.* $2 \cdot 10^4$ configuration state functions (CSF) were selected for the lowest eight states in each symmetry in the D_2 subgroup (12 for A symmetry, six states for each symmetry in the triplet case). The number of reference configurations was 110 and 74 in both the singlet and triplet calculations, respectively. The oscillator strengths (*f*) were obtained from the dipole-lengths form. All DFT-MRCI calculations were performed in the D_2 subgroup of the full D_{2d} point group of **1**.

Finally, we resorted to a recently introduced molecular density functional method based on time-dependent (TD) response theory [42]. Analogous to *Hartree-Fock* TD response theory (*e.g.* in the *Tamm-Dancoff* or random-phase approximation), the poles and the residues of the frequency-dependent polarizability are evaluated, where the former correspond to vertical excitation energies and the latter to oscillator strengths. Also analogous to TD-HF, excited states are then described in the basis of all possible single excitations, which makes for a very transparent interpretation of the results. However, although the treatment of electron correlation in TD density functional response theory (TD-DFT) goes far beyond that in a HF-based CIS method. However, double excitations are not taken into account explicitly, which makes that excited states that are dominated by such excitations cannot be modelled correctly.

We used the TD-DFT implementation in Gaussian 98 [32] as described recently by *Stratmann et al.* [43][5]), together with the 6-31G* basis set. The MOs in *Fig. 1* were plotted with the MOPLOT program [44] which gives a schematic representation of the MO's nodal structure within a ZDO-type approximation [45].

Supporting Information. Cartesian coordinates and energies of **1** and its radical ions, and detailed results of excited-state calculations are available from the authors.

REFERENCES

[1] H. E. Simmons, T. Fukunaga, *J. Am. Chem. Soc.* **1967**, *89*, 5208.
[2] R. Hoffmann, A. Imamaura, D. G. Zeiss, *J. Am. Chem. Soc.* **1967**, *89*, 5215.
[3] F. Steuber, J. Staudigel, M. Stösel, J. Simmerer, A. Winnacker, H. Spreitzer, F. Weisstörtel, J. Salbeck, *Adv. Mater.* **2000**, *12*, 130.
[4] M. F. Semmelhack, J. S. Foos, S. Katz, *J. Am. Chem. Soc.* **1972**, *94*, 8637.
[5] M. F. Semmelhack, J. S. Foos, S. Katz, *J. Am. Chem. Soc.* **1973**, *95*, 7325.
[6] C. Batich, E. Heilbronner, E. Rommel, M. F. Semmelhack, J. S. Foos, *J. Am. Chem. Soc.* **1974**, *96*, 7662.
[7] M. F. Semmelhack, H. N. Weller, J. S. Foos, *J. Am. Chem. Soc.* **1977**, *99*, 292.
[8] T. Haumann, J. Benet-Buchholz, R. Boese, *J. Mol. Struct.* **1996**, *374*, 299.
[9] R. Gleiter, J. Spanget-Larsen, in 'Advances in Strain in Organic Chemistry', Ed. B. Halton, JAI Press Ltd., London, 1992, p. 143.
[10] M. D. Gordon, T. Fukunaga, H. E. Simmons, *J. Am. Chem. Soc.* **1976**, *98*, 8401.
[11] J. Kao, L. Radom, *J. Am. Chem. Soc.* **1978**, *100*, 760.
[12] D. P. Craig, P. J. Stiles, P. Palmieri, C. Zauli, *J. Chem. Soc., Faraday Trans. 2* **1979**, *75*, 97.
[13] V. Galasso, *Chem. Phys.* **1991**, *153*, 13.
[14] P. Forster, R. Gschwind, E. Haselbach, U. Klemm, J. Wirz, *Nouv. J. Chim.* **1980**, *4*, 365.
[15] E. Haselbach, U. Klemm, R. Gschwind, T. Bally, L. Chassot, S. Nitsche, *Helv. Chim. Acta* **1982**, *65*, 2464.
[16] A.-C. Sergenton, Thesis No. 1375, University of Fribourg, 2000.
[17] C. Bulliard, M. Allan, J. M. Smith, D. A. Hrovat, W. T. Borden, S. Grimme, *Chem. Phys.* **1997**, *225*, 153.
[18] C. Bulliard, M. Allan, G. Wirtz, E. Haselbach, K. A. Zachariasse, N. Detzer, S. Grimme, *J. Phys. Chem. A* **1999**, *103*, 7766.
[19] C. Bulliard, M. Allan, S. Grimme, *Int. J. Mass. Spectrom.* **2001**, *205*, 43.
[20] M. Allan, *J. Electron Spectrosc. Relat. Phenom.* **1989**, *48*, 219.
[21] T. Bally, S. Nitsche, K. Roth, E. Haselbach, *J. Am. Chem. Soc.* **1984**, *106*, 3927.
[22] D. Chen, G. A. Gallup, *J. Chem. Phys.* **1990**, *93*, 8893.
[23] S. T. Brown, J. C. Rienstra-Kiracofe, H. F. Schaefer, *J. Phys. Chem. A* **1999**, *103*, 4065.
[24] T. Bally, S. Nitsche, K. Roth, *J. Chem. Phys.* **1986**, *84*, 2577.
[25] L. Truttmann, K. R. Asmis, T. Bally, *J. Phys. Chem.* **1995**, *99*, 17844.
[26] M. Allan, *Helv. Chim. Acta* **1982**, *65*, 2008.
[27] K. R. Asmis, M. Allan, *J. Phys. B* **1997**, *30*, 1961.
[28] T. Bally, in 'Radical Ionic Systems', Eds. A. Lund and M. Shiotani, Kluwer, Dordrecht, 1991, p. 3.
[29] T. Shida, 'Electronic Absorption Spectra of Radical Ions', Elsevier, Amsterdam, 1988.
[30] A. D. Becke, *J. Chem. Phys.* **1993**, *98*, 5648.
[31] C. Lee, W. Yang, R. G. Parr, *Phys. Rev. B* **1988**, *37*, 785.
[32] M. J. Frisch, G. W. Trucks, H. B. Schlegel, G. E. Scuseria, M. A. Robb, J. R. Cheeseman, V. G. Zakrzewski, J. A. Montgomery, R. E. Stratmann, J. C. Burant, S. Dapprich, J. M. Millam, A. D. Daniels, K. N. Kudin, M. C. Strain, O. Farkas, J. Tomasi, V. Barone, M. Cossi, R. Cammi, B. Mennucci, C. Pommelli, C. Adamo, S. Clifford, J. Ochterski, G. A. Petersson, P. Y. Ayala, Q. Cui, K. Morokuma, D. K. Malick, A. D. Rabuck, R. Raghavachari, J. B. Foresman, J. Cioslowski, J. V. Ortiz, B. B. Stefanov, G. Liu, A. Liashenko, P. Piskorz, I.

---

[5]) The transition moments that appear in the TD-DFT output of Gaussian should probably be taken with a grain of salt because their absolute values vary by orders of magnitude depending on the number of excited states (NStates = nn) that are calculated.

Komaromi, R. Gomperts, R. L. Martin, D. J. Fox, T. Keith, M. A. Al-Laham, C. Y. Peng, A. Nanayakkara, M. Challacombe, P. M. W. Gill, B. G. Johnson, W. Chen, M. W. Wong, J. L. Andres, C. Gonzales, M. Head-Gordon, E. S. Repogle, J. A. Pople, 'Gaussian 98, Rev. A1', Gaussian, Inc., Pittsburgh, PA, 1998.

[33] B. G. Johnson, P. M. W. Gill, J. A. Pople, *J. Chem. Phys.* **1993**, *98*, 5612.

[34] K. Andersson, B. O. Roos, in 'Modern Electronic Structure Theory', World Scientific Publ. Co., Singapore, 1995, Vol. 2, Part 1, p. 55.

[35] K. Andersson, M. R. A. Blomberg, M. P. Fülscher, V. Kellö, R. Lindh, P.-Å. Malmqvist, J. Noga, J. Olson, B. O. Roos, A. Sadlej, P. E. M. Siegbahn, M. Urban, P.-O. Widmark, 'MOLCAS, Version 4', University of Lund, Sweden, 1998.

[36] K. Pierloot, B. Dumez, P.-O. Widmark, B. O. Roos, *Theor. Chim. Acta* **1995**, *90*, 87.

[37] S. Grimme, M. Waletzke, *J. Chem. Phys.* **1999**, *111*, 5645.

[38] R. Ahlrichs, M. Bär, M. Häser, H. Horn, C. Kölmel, *Chem. Phys. Lett.* **1989**, *162*, 165.

[39] O. Treutler, R. Ahlrichs, *J. Chem. Phys.* **1995**, *102*, 346.

[40] A. Schäfer, C. Huber, R. Ahlrichs, *J. Chem. Phys.* **1994**, *100*, 5829.

[41] A. D. Becke, *J. Chem. Phys.* **1993**, *98*, 1372.

[42] M. E. Casida, in 'Recent Advances in Density Functional Methods, Part I', Ed. D. P. Chong, World Scientific, Singapore, 1995, p. 155.

[43] R. E. Stratmann, G. E. Scuseria, M. J. Frisch, *J. Chem. Phys.* **1998**, *109*, 8218.

[44] T. Bally, B. Albrecht, S. Matzinger, M. G. Sastry, 'MOPLOT, a Program for Displaying Results of LCAO-MO Calculations, Version 3.2', available on request from thomas.bally@unifr.ch, University of Fribourg, 1997.

[45] E. Haselbach, A. Schmelzer, *Helv. Chim. Acta* **1979**, *54*, 1299.